atmosphere

MDPI

Article

Characteristics of Indoor and Soil Gas Radon, and Discussion on High Radon Potential in Urumqi, Xinjiang, NW China

Nanping Wang [1,*], Jingming Yang [2], Haochen Wang [2], Binlin Jia [1] and Aimin Peng [1]

[1] School of Geophysics and Information Technology, China University of Geosciences (Beijing), 29 Xueyuan Road, Beijing 100083, China
[2] Geologic Party No. 216, China National Nuclear Corporation, 467 Beijing South Road, Urumqi 830011, China
* Correspondence: npwang@cugb.edu.cn

Abstract: Urumqi City, located in the northwest of China, is a city with a high indoor radon concentration in a nationwide indoor radon survey in China. This study focuses on the assessment of the indoor radon level and its distribution in this city. Indoor radon measurement using RAD7 and solid nuclear track detector (SSNTD), soil gas radon measured by RAD7, and the determination of the specific activity of uranium and radium in soil samples by a high pure germanium spectrometer were performed from 2021 to 2023. The results reveal a wide range of indoor radon concentrations in Urumqi, with anomalies above 400 Bq/m^3 in some dwellings. The arithmetical and geometric mean values of indoor radon concentration are 80 ± 77 Bq/m^3 and 58 Bq/m^3, respectively. The geometric mean value of radon measured by SSNTD is 101 Bq/m^3. The distribution of areas with a high indoor radon concentration is spatially consistent with deep and large active faults or overlapping and intersection zones of multiple groups of faults. It is recommended to conduct a more comprehensive investigation and research into the elevated radon potential and radioactivity associated with building materials.

Keywords: indoor radon; radon potential; faults; earthquake; Urumqi

Citation: Wang, N.; Yang, J.; Wang, H.; Jia, B.; Peng, A. Characteristics of Indoor and Soil Gas Radon, and Discussion on High Radon Potential in Urumqi, Xinjiang, NW China. *Atmosphere* **2023**, *14*, 1548. https://doi.org/10.3390/atmos14101548

Academic Editors: Qiuju Guo, Miroslaw Janik and Boris Igor Palella

Received: 24 July 2023
Revised: 8 October 2023
Accepted: 9 October 2023
Published: 11 October 2023

1. Introduction

Radon (^{222}Rn) is a radioactive gas generated from the decay of uranium radioactive series. Inhaling radon radioactive gas and its short-lived decay progenies can damage the respiratory system and increase the incidence of lung cancer. The excess relative risk (ERR) and lung cancer risk due to continuous exposure to high radon concentrations in the home are comparable to those of miners, indicating a correlation between lung cancer risk and residential radon exposure [1–3]. Global cancer statistics and cancer research reports in China have shown that lung cancer has the highest incidence and mortality rate among malignant tumors [4,5].

Since the late 1970s, extensive research has been conducted worldwide on indoor radon and radon geological potential. It has been found that houses with high radon concentrations are mostly located in areas with high radon geological potential. The indoor radon concentration in a region is related to factors such as near-surface lithology, soil permeability, and geological structures [6–10].

Due to its large land area and budget constraints, China has not yet conducted a detailed national indoor radon assessment project, and research on radon potential mapping in China is generally insufficient. Since the late 1980s, studies have been conducted on radon and lung cancer, radon potential, and indoor radon levels in areas with high radon geological potential in southern China, such as Yangjiang, Shenzhen, Zhuhai in Guangdong Province, and Gejiu in Yunnan Province [11–15]. In Guangdong, the high indoor radon levels are mainly due to the widespread occurrence of Yanshanian period biotite granite with high uranium, radium, and thorium contents, while in Gejiu, it is mainly caused by the

fragmentation of tin ore rocks and tin mining, resulting in high indoor radon and thoron concentrations [16,17]. In addition, studies have been conducted on radon and thoron concentrations in cave dwellings in Qingyang and Pingliang in Gansu Province [18–20].

Until now, four nationwide indoor radon surveys have been conducted in China. From the mid-1980s to 1994, the indoor radon survey was carried out in more than 9000 dwellings nationwide, and the arithmetic mean (AM) of the indoor radon concentration was 23.7 Bq/m^3 [21,22], mainly measured using grab sampling with a scintillation chamber. From 2001 to 2004, long-term cumulative measurements of indoor radon were conducted in 20 cities and six counties using a solid-state nuclear track detector (SSNTD), with a sampling number of 3098 homes. The survey results showed that the indoor radon concentration in urban areas of China had increased. The AM and geometric mean (GM) of the indoor radon concentration were 43.8 ± 37.7 Bq/m^3 and 37.4 Bq/m^3, respectively. The number of rooms exceeding 100, 200, and 400 Bq/m^3 accounted for 6.4%, 0.7%, and 0.06% of the total surveyed rooms, respectively [13,23]. Higher indoor radon concentrations were also detected in areas such as Shangrao City in Jiangxi Province and Urumqi City in Xinjiang Autonomous Region [24]. The fourth national indoor radon survey was performed from 2006 to 2010 using the SSNTD method, covering 2029 households. The weighted mean concentration was 32.6 ± 5.2 Bq/m^3, and the percentage of rooms with a radon concentration exceeding 100 Bq/m^3 (36 rooms) accounted for 1.8% of the total surveyed rooms [25,26]. The annual average indoor radon concentration in Urumqi was 57 Bq/m^3, indicating a relatively high level compared to the national average [25,27,28].

However, in terms of geological background, Urumqi should not be a high radon potential area. In Urumqi, apart from geological faults and earthquakes, the lithology uranium and radium content of the soil should not be the main influencing factors in high indoor radon concentrations.

According to the data from a 1:250,000 scale multi-target regional geochemical survey in the Urumqi–Changji area, uranium and thorium were evenly distributed in surface soil samples in Urumqi, with contents of 2.53 ± 0.13 ppm and 9.21 ± 0.08 ppm, respectively. The differences in uranium and thorium concentrations among different geological formations are not significant [29]. Moreover, the soil radon concentration in Urumqi was relatively low, with an average value of 3288 Bq/m^3 and a range of 45–41,164 Bq/m^3, much lower than the nationwide average of 9614 Bq/m^3 in 18 cities [30].

Since both soil uranium content and soil radon concentration are lower than the national average, what makes Urumqi one of the few cities in China with a high indoor radon concentration? In order to understand the distribution and characteristics of indoor radon concentration in Urumqi, we conducted indoor radon and soil radon measurements, as well as measuring the uranium and radium radioactivity concentration in soil samples, in typical geological structures and densely populated areas of Urumqi from 2020 to 2023, aiming to identify the causes of high radon potential in Urumqi.

2. Materials and Methods

2.1. Radon Measurement

2.1.1. Instantaneous Radon Measurement

In the instantaneous measurement of indoor radon and soil gas, a RAD7 (DURRIDGE Company Inc., Billerica, MA, USA) device with silicon semiconductor was adopted.

In this radon survey, the instantaneous radon measurement was carried out in accordance with the guiding method of radon concentration measurement in GB/T 18883-2022, China's national standard for indoor air quality [31]. Doors, windows, and ventilation systems should be closed for more than 12 h before the radon measurement.

The radon measurement was performed in the living room or bedroom of apartments or houses, as well as in offices. All the buildings were made of concrete, most of them were multi-storey apartments, some were three-storey houses and some were built on hills. Radon measurements were also carried out in the basement, even though basements are storage rooms, not living rooms in Urumqi. The indoor radon monitoring was generally

carried out on the 1st to 3rd floor. The average altitude of Urumqi is 800 m, and more than 50% of the area of Urumqi is mountainous. Therefore, there are certain differences in the elevation of buildings in different regions.

In the indoor radon measuring, the RAD7 was set to normal mode with a 1 h sampling time, and was placed on a table in the living room or on a desk in the bedroom at a height of 60–80 cm above the ground and at a distance of more than 30 cm from the wall.

In the investigation of radon in soil gas, the RAD7 was set to sniff mode with a sampling time of 3 min. The soil gas sampling depth was 80 cm below the ground, and the hole was sealed with soil [32,33].

An Alpha GUARD (PQ2000) served as a reference for comparison measurements and quality control at some indoor radon measuring sites. The instrument was set to flow mode with a sampling time of 10 min.

All of the instruments were calibrated annually at the Radon Chamber of the National Institute of Metrology, China.

2.1.2. Long-Term Radon Measurement

The long-term measurements using passive integrated radon–thoron discriminative detectors were carried out by an LD-P detector, a kind of solid-state nuclear track detector (SSNTD). The detector consisted of two diffusion cups for both ^{222}Rn and ^{220}Rn, with two built-in CR-39 films produced by Japan's FUKUVI Chemical Company [34]. Prior to use, the detector was calibrated at the University of South China.

During the investigation, the LD-P detectors were affixed to the periphery of a writing desk or a closet within the bedroom. They were positioned at distances of 5 cm from the wall and at heights of 80–90 cm above the floor. This deployment spanned a period of 90 days, spanning from January to April during the winter season.

According to the procedure set out in GB/T 18883-2022 for long-term radon measurement sampling time and sampling period, SSNTD sampling was selected to be carried out in winter, and the radon detector exposure time was not less than 90 days.

Following the 90-day exposure interval, the LD-P detectors were subjected to dissolution using a solution of 6.25 mol/L NaOH, maintained at a temperature of 80 °C for a duration of 8 h. The resulting etched tracks on each LD-P detector were subsequently examined through manual observation utilizing a microscope. Initially, a preliminary assessment was conducted to evaluate the uniformity of the CR-39 tracks. The region in the center of the track plate, characterized by a more consistent track density, was generally chosen as the designated observation area. Subsequently, systematic observation was conducted by moving the CR-39 slide horizontally, recording the number of tracks within each field of view. Each observed field of view encompassed an area of 0.7854 mm^2, corresponding to a circular region with a diameter of 1 mm. A total of 40 fields of view were documented. Furthermore, the track density of each detector was determined by calculating the average number of tracks across the 40 observed fields of view. Ultimately, the radon concentrations at the monitored sites were computed with an appropriate conversion factor.

The process of etching, reading the nuclear tracks of the CR-39 slides, and calculating the radon concentrations using the LD-P detectors were performed in the laboratory of the Institute of Radiation Protection and Nuclear Safety Medicine, Chinese Center for Disease Control and Prevention.

2.2. Indoor Gamma Spectrometry and Dose Rate Measurement

In order to understand the relationship between the indoor radon concentration and the radionuclide content of the building materials, a portable BGO detector gamma spectrometer (GF Instruments, s.r.o., in Brno, Czech Republic) was used to determine the content of uranium, thorium, and potassium, and the gamma-ray dose rate.

During indoor measurement, the instrument was placed on a wooden support in the center of the room and the detector was set at a height of 100 cm above the ground. Each

gamma spectrum data acquisition took 3 min and an average of 5 measurements was taken as the measured result at each site.

2.3. Soil Sample Collection

Soil samples were collected at the locations where the soil radon measurements were taken. Soil sample collection uses a ring knife sampler, which consists of a cylindrical ring knife with a blade at one end (hollow cylinder with a diameter of 70 mm and a height of 52 mm), an aluminum box, and a metal cover with a handle. The sampling steps are as follows:

(1) Clean the sampling site and remove weeds, dead branches, and rubble;
(2) Press the edge of the ring knife vertically down or hit the ring knife into the soil with a hammer until the ring knife barrel is filled with a soil sample;
(3) Use a paring knife to cut the soil around the ring knife, take out the ring knife that has been filled with soil, cut off the soil at both ends of the ring knife, and immediately cover the two ends of the ring knife and put it into an aluminum box, or tip the contents into a plastic bag.

2.4. Determination of Specific Activity of Radionuclides in Soil

The specific activity of radionuclides, including uranium, radium, thorium, and cesium, present in the soil samples was determined using a HPGe digital wide-energy gamma-ray spectrum measurement system made by CANBERRA. The detector model is BE3830, and its energy resolution for ^{60}Co is 1.68 keV (for 1332.5 keV energy peak). The detector of the spectrometer is placed in a 10 cm thick lead chamber with a relative detection efficiency of 50%. The extended uncertainties for uranium (63.3 and 92.4 keV), radium (351.9 and 609.3 keV), thorium (583.2 and 911.2 keV), and cesium (661.7 keV) were 5.6%, 5.0%, 5.4%, and 4.1%, respectively. The device was calibrated using a volume reference source (φ 75 × 70 mm) mixed with radionuclides of ^{238}U, ^{232}Th, ^{40}K, ^{60}Co, and ^{137}Cs, provided by the National Institute of Metrology, China.

After being transported to the laboratory, the sample was pretreated and analyzed following the guidance of the "Gamma-ray spectrometry method for the determination of radionuclides in environmental and biological samples" [35]. After the samples were dried at 105 degrees and sealed for 3–4 weeks, the specific activities of the uranium, radium, thorium, and cesium were determined by a HPGe wide-energy gamma spectrometer. The spectral data collection time was 12 h.

2.5. Geological Overview of the Study Area and Sampling Site Selection

2.5.1. Geographic and Climatic Features

Urumqi City is located between 86°37′33″ and 88°58′24″ east longitude and 42°45′32″ and 45°00′00″ north latitude in the northwest of China. Urumqi is situated at the northern foot of the Tianshan Mountains on the southern edge of the Junggar Basin, with mountains on three sides and more than 50% of its total area being mountainous terrain. The northern part consists of a small alluvial plain, which accounts for less than one-tenth of the total area. The city has a permanent population of 4.0824 million people [36].

Urumqi City has a temperate continental climate with semi-arid characteristics. The hottest months are July and August, with an average temperature of 25.7 °C. The coldest month is January, with an average temperature of −15.2 °C. Summers are hot and dry, while winters are cold and long [37].

2.5.2. Geological Overview

The main exposed strata in Urumqi are Upper Carboniferous, Permian, Triassic, Jurassic, Cretaceous, Tertiary, and Quaternary, and their lithology mainly includes sandstone, siltstone, conglomerate, and mudstone, while the Quaternary sediments are mainly alluvial gravel, silty sand, and sandy soil.

Due to its location at the junction of the Bogda Arcuate Uplift Belt and the Urumqi Mountain Front Depression at the southern edge of the Junggar Basin, Urumqi City is characterized by the convergence of multiple tectonic belts, resulting in complex geological structures and intense tectonic activity. The region is prone to frequent moderate to strong earthquakes. Major fault systems in the area include near-east–west trending faults (the Fukang South Fault and the Xishan Fault), north–east faults (the Yamalike-Shuimogou Fault, the Wanyao Gou Fault, and the Bagang-Shihua Concealed Fault), as well as the near-north–south trending concealed faults related to the Urumqi River [38–41]. A simplified geological map of Urumqi City (1:10,000) with the location of radon measurements is shown in Figure 1.

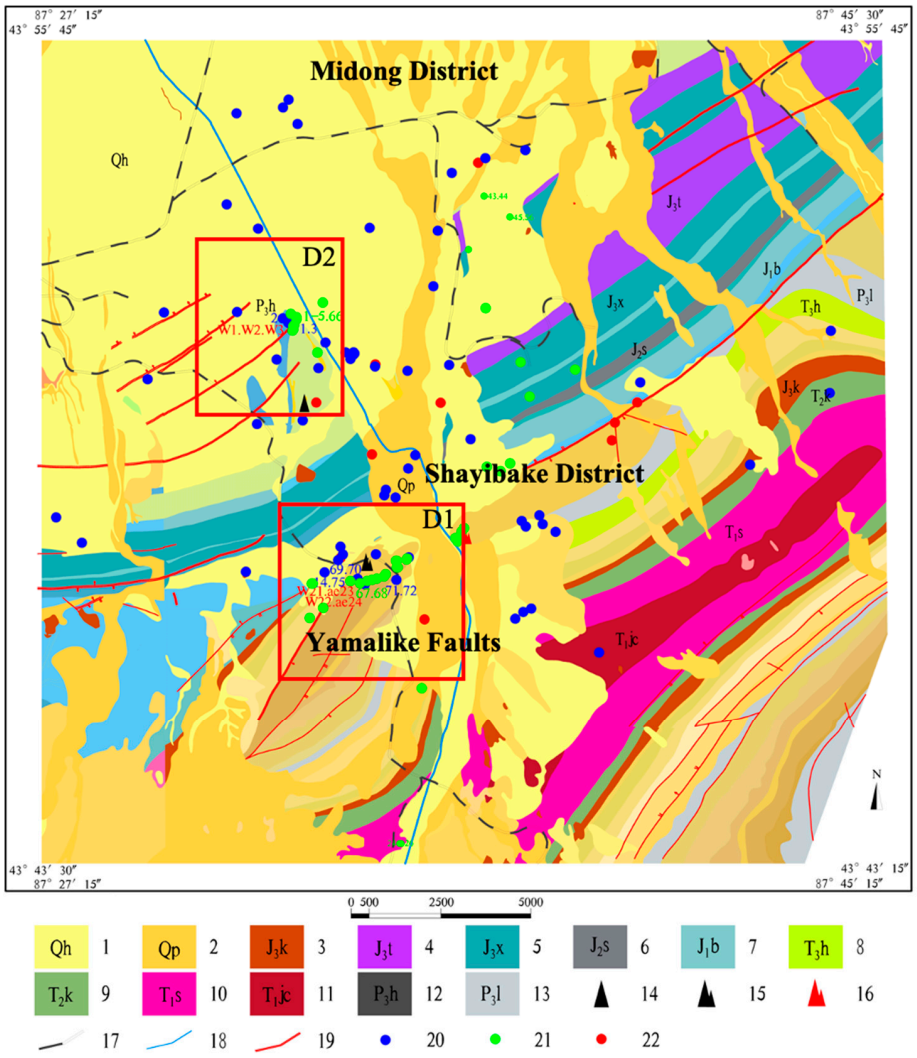

Figure 1. A simplified geological map of Urumqi City (1:10,000) with location of radon measurements: 1—Qh: sandy gravel layer interbedded with fine sand and silty clay; 2—Qp: Gravel, sand, silt, clay; 3—J_3k Kalazha Formation: reddish brown sandstone; 4—J_3t Toutunhe Formation: purple iron argillaceous siltstone; 5—J_2x Xishanyao Formation: mudstone; 6—J_2s Sangonghe Formation: sandstone; 7—J_1b Badaowan Formation: sandstone; 8—T_3h Huangshanjie Formation: sandstone and mudstone; 9—T_2k Karamay Formation: sandstone and mudstone; 10—T_1s Shaofanggou Formation: glutenite and mudstone; 11—T_1jc Jiucaiyuan Formation: mudstone and sandstone; 12—P_3 Hongyanchi Formation: argillaceous siltstone; 13—P_3l Lucaogou Formation: calcareous siltstone; 14—Zhizhu Hill; 15—Yamalike Mountain; 16—Hongshan Hill; 17—Railway; 18—Heping channel; 19—Measured faults; 20—Indoor radon survey location; 21—Soil radon sampling site; 22—Long-term radon monitoring location.

2.5.3. Radon Sampling Site Selection

Based on the comprehensive study of the geological, tectonic, and surface sediment characteristics in Urumqi, we did not employ a grid sampling approach. Instead, we focused on selecting radon survey sites in the areas where geological faults are active, including the Yamalike-Shuimogou Fault, the concealed fault in Wanyao Gou, and the southern Hongshan Fault, as well as the vicinity of Yamalike Mountain and Zhizhu Hill located in the geochemical uranium anomalies belt. Indoor radon and soil radon surveys should be carried out in areas where the soil is not disturbed as far as possible. In order to compare the measurement results, some indoor radon survey sites were also selected in other regions, as shown in Figure 1.

3. Results

3.1. Indoor Radon Characteristics

From 2020 to 2023, a total of 151 instantaneous radon measurements using RAD7 and 32 cumulative radon measurements using SSNTD were conducted. Of the 151 measured data, 40 were measured in the basement and 111 on other floors. If the same measurement site had been measured multiple times, its value was the arithmetic average of the multiple measurement results. Therefore, 97 effective measurement data were obtained in this survey, including 23 in the basement and 74 on other floors.

Instantaneous measurements were mainly carried out in winter, some measurement sites were completed in summer, and the SSNTD was implemented in winter. In instantaneous measurement, the RAD7 adopts the normal mode of 24 h continuous measurement.

The sampling sites were primarily located in residential buildings and offices in densely populated areas of Xinshi District, Tianshan District, Shuimogou District, and Shayibake District. When conducting measurements in residential or office buildings, radon concentrations in the basements were measured simultaneously whenever possible.

3.1.1. Instantaneous Radon Concentrations

Statistical methods were used to process the measured data, and the anomalous value of indoor radon concentration was executed by the Pauta Criterion with the assistance of SPSS. The same method was also applied to the data processing for both the SSNTD and the soil radon measurements (Sections 3.1.2 and 3.3).

The statistics of a total of 94 measurements detected by the RAD7 radon monitor, excluding three anomalous points, are listed in Table 1. Table 1 demonstrates a significant variation of radon concentrations in both the indoor and basement sites.

Table 1. Indoor radon concentration measurement by RAD7 (Bq/m^3).

Location	N	AM	SD	MIN	MAX	MED	GM
Indoors	71	80	77	9	435	57	58
Basement	23	297	254	28	961	227	202

Out of the 74 radon survey locations, there were 17 measurement sites where indoor radon concentrations surpassed 100 Bq/m^3, 4 sites where it exceeded 200 Bq/m^3, and 2 sites where it exceeded 300 Bq/m^3. These figures represent 23.9%, 5.6%, and 2.8% of the total number of buildings investigated, respectively (Figure 2a). Because several high values of radon were observed, the AM value is higher than the GM value. In Table 1, the highest radon concentration (435 Bq/m^3) of the indoor samples was measured in the area of Yamalike Mountain, in a site located on the first floor. The current indoor radon limit standard in China is the "Standard of Indoor Air Quality" GB/18883-2022 ($\leq$300Bq/m^3), which means that 2.8% of the houses in Urumqi exceed the action level, and a detailed indoor radon assessment is needed to determine whether radon reduction actions are needed.

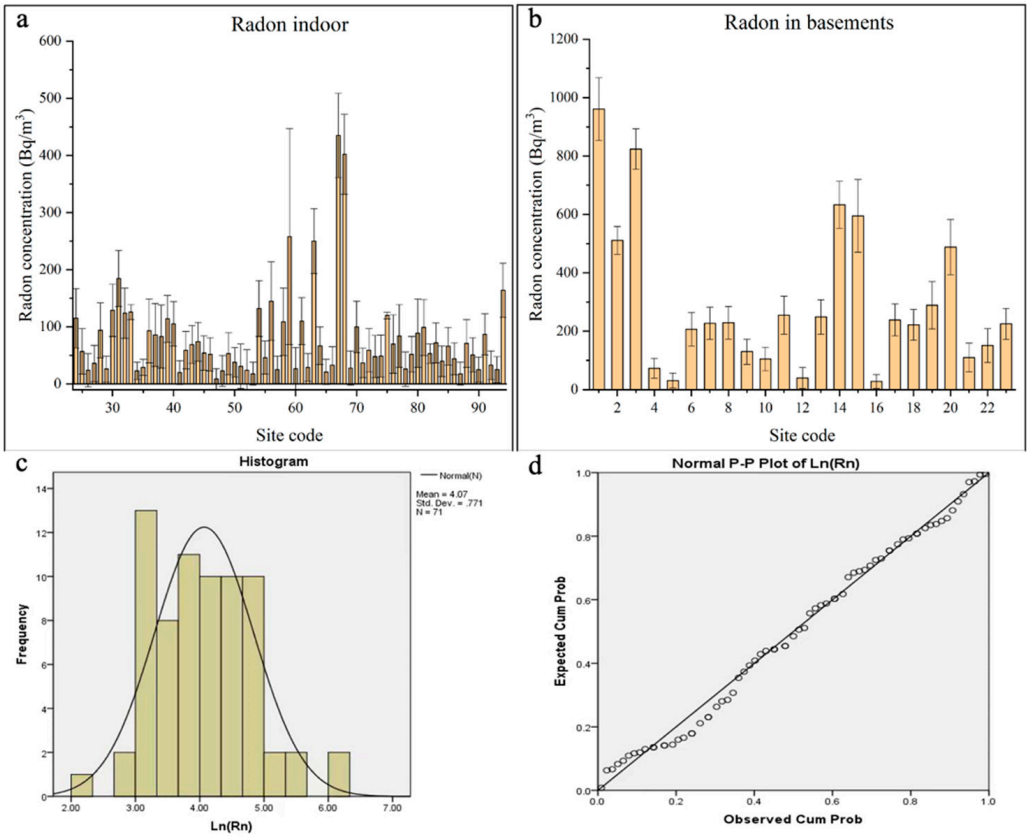

Figure 2. Measured radon concentration in indoor areas: (**a**) indoor Rn, (**b**) Rn in basements, (**c**) the statistical histogram of radon in indoor areas, (**d**) normal P-P plot of radon indoor.

The AM of the indoor Rn concentrations at the 71 sites is 80 ± 77 Bq/m^3, ranging from 9 to 435 Bq/m^3, with the median and GM being 57 and 58 Bq/m^3, respectively. The data on indoor radon measurements present a lognormal distribution pattern, shown in Figure 2c,d.

Three indoor radon anomalies were also observed there, and instantaneous radon measurements exceeding 3000 Bq/m^3 were observed in three houses, one of which was inspected using the SSNTD method, and the two measurement results (by RAD7 and by SSNTD) were generally consistent (see Section 3.1.2). These indoor radon anomalies are located near the Yamalike active fault, where several secondary faults are also developing. These anomalous buildings are made of concrete, built on a hillside of Yamalike Mountain.

The monitored radon concentration in the basements is generally high, and the AM, median, and GM are all greater than 200 Bq/m^3 (Table 1). In April 2021, instantaneous radon concentrations above 1000 Bq/m^3 were also observed in two basements of two buildings located near the intersection of the east–west and north–south fractures in Zhizhu Hill. The two buildings are of the same type, both concrete high-rise buildings (apartments), but the indoor radon concentration in the basements varied in the range of 37 to 588 Bq/m^3 in September and November 2020. This is an unconformity contact area of the Qizigou Formation under the Karaza Formation in the Lower Jurassic, where uranium is locally enriched in the Qingshuihe Formation. The variation of radon concentration in the basements may be affected by the stratum contact zone and underground fault. Installing air ventilation in the basements will greatly reduce the radon concentration in the basements. The increased ventilation rate in summer and autumn is also an effective factor to reduce indoor radon concentration.

The statistical summaries of the indoor radon concentrations in each district are listed in Table 2. The measured radon data in Shayibake District are highly discrete, and the AM is the highest (109 ± 120 Bq/m^3). The three indoor radon anomalies are all distributed in

the Shayibake District, located in the middle of Urumqi (D1 in Figure 1). The Yamalike Faults pass through the middle of Shayibake District. The AM in Midong District was the lowest (59 ± 33 Bq/m^3) (located in the north of Figure 1), and the surface soil was mainly covered by Quaternary sediment, where faults were not developed.

Table 2. Statistics of indoor radon concentrations in each district (Bq/m^3).

District	N	AM	SD	MIN	MAX	MED	GM
Xinshi District	26	72	43	9	186	64	59
Shayibake District	22	109	122	18	435	52	66
Tianshan District	8	59	33	20	120	51	51
Toutunhe District	4	78	20	53	99	80	76
Midong District	4	42	20	18	66	42	38
Shuimogou District	7	65	50	25	164	51	52

3.1.2. Long-Term Cumulative Radon Measurements

To assess the reliability of the instantaneous radon measurements in Urumqi, long-term cumulative radon measurements (using SSNTD) were conducted for a three-month period in the winters of 2022 and 2023. Out of the 32 measurement points, 50% of them were subjected to instantaneous measurements using the RAD7. The comparative results are shown in Figure 3. The median values obtained using the SSNTD and RAD7 are 79 Bq/m^3 and 123 Bq/m^3, respectively. The median value of 16 samples (79 Bq/m^3) is equal to that of 21 samples, as shown in Table 3.

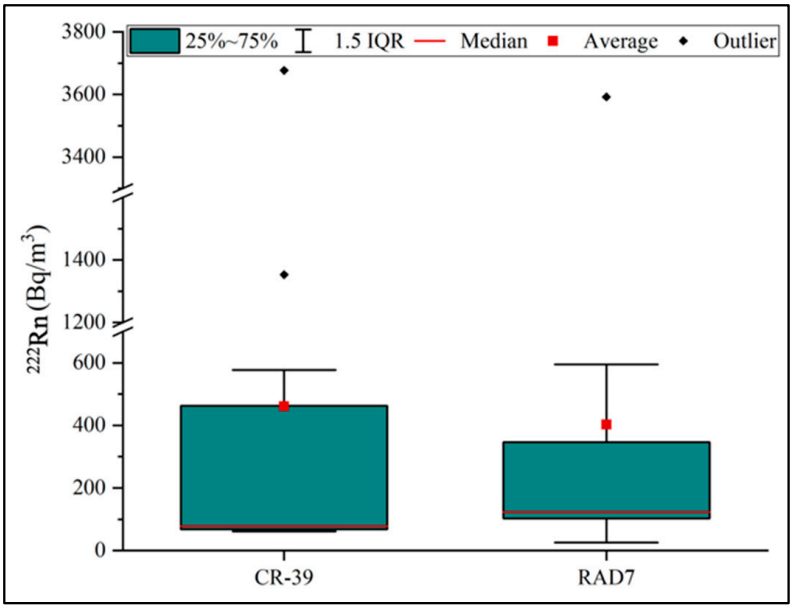

Figure 3. Comparison of radon concentrations by SSNTD and RAD7.

Table 3. Indoor radon concentration measurement by SSNTD (Bq/m^3).

Location	N	AM	SD	MIN	MAX	MED	GM
Basement	9	307	337	33	1080	185	174
Indoors	21	150	179	31	685	79	101

Table 3 presents the statistical data for the 31 measurements of indoor radon concentrations determined using the SSNTD, and one outlier (3677 Bq/m^3) was not counted. This outlier (3677 Bq/m^3) is approximately the result of the instantaneous radon measurements (3592 Bq/m^3), as shown in Figure 3. However, due to the small number of samples

measured by the SSNTD method, the high radon concentration value accounts for a large proportion, and its arithmetic and geometric mean values are higher than those of the RAD7. In addition, we also need to pay attention to the uncertainty of these two methods. The uncertainty of the LD-P detectors related to the sampling period and the radon level in the environment: the typical uncertainty was 10–25% for 200 Bq/m^3 for an optimal exposure period. The uncertainty of the RAD7 was perhaps 30–50% when the indoor radon concentration was below 50 Bq/m^3. The comparison between the measured values of the SSNTD and RAD7 is shown in Figure 3, but the median of the SSNTD is lower than that of the RAD7.

According to the indoor radon concentration measurement method recommended by the "Standard of indoor air Quality" GB/T 18883-2022 for the SSNTD, the indoor radon concentration should be measured for at least 3 months (including in the winter season). Therefore, our SSNTD survey was carried out in the winter season. In addition, due to the cold climate in Urumqi City, the winter lasts for half of the year (with heating supplied from 15 October to 15 April), so the measurement results are representative.

In summer, doors and windows are often opened. With the increase in the indoor and outdoor ventilation rate, the indoor radon concentration is expected to decrease. In the cold areas of northeast China, indoor radon concentration is significantly higher in winter than in summer [42].

3.1.3. Indoor Radon and Building Age

The measured indoor radon data were statistically analyzed according to the construction time of the building, and the results are shown in Figure 4. The statistical period was 10 years, and the results were the arithmetical average of the indoor radon concentration in all the buildings every 10 years. Figure 4 shows that the average indoor radon concentration was the highest in the 1960s and the lowest in the 1980s. Although the indoor radon concentration has increased since 2000, the difference is not obvious. In the past 20 years, the indoor radon concentration in newly built residential buildings in China has increased [25,43], mainly because the tightness of the doors and windows has been greatly improved.

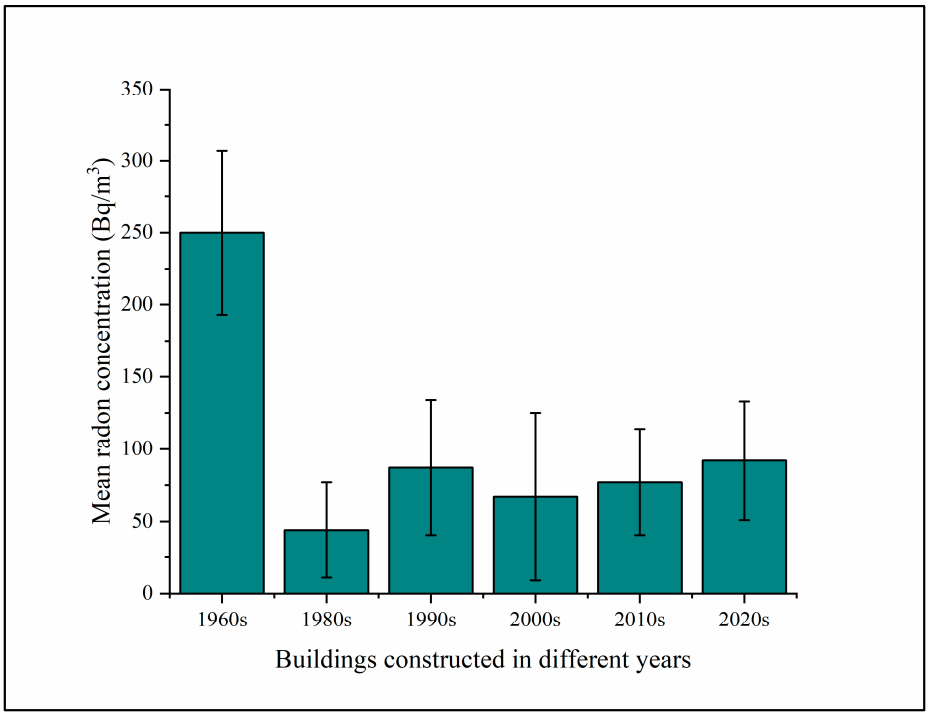

Figure 4. Mean radon concentration in buildings constructed in different years.

The high indoor radon concentration in buildings is related to their geographical location. The dwellings with an indoor radon concentration greater than 200 Bq/m^3 are mainly distributed in the fault-developed areas, such as Yamalic Mountain and Zhizhu Hill, and there is no obvious relationship with the construction age of the buildings. The residential buildings in Urumqi are mainly high-rise buildings, and the number of villa houses in our investigation accounts for only 8% of the total number of buildings. There is no relationship between residential houses with a high indoor radon concentration and abnormal points and the building type.

3.2. Specific Activities of Uranium, Radium, and Cesium in Soil

Table 4 presents the statistical results of the specific activities of the uranium (^{238}U), radium (^{226}Ra), thorium (^{232}Th), potassium-40 (^{40}K), and cesium (^{137}Cs) in the 45 soil samples from Urumqi.

Table 4. Uranium, radium, thorium, potassium-40, and cesium radioactivity specific activities (Bq/kg).

	^{238}U	^{226}Ra	^{232}Th	^{40}K	^{137}Cs	k/(U/Ra) *
N	45	45	45	45	30	44
AM	41	45	41	855	4.42	1.01
SD	9	14	5	49	5.83	/
MIN	22	27	26	757	0.14	/
MAX	72	104	48	967	26.74	/

* k is the radioactive equilibrium coefficient of uranium and radium.

From Table 4 and Figure 5, the following observations can be made:

1. The distribution of ^{238}U, ^{226}Ra, ^{232}Th, and ^{40}K in the soil samples is generally uniform. The distribution trends of ^{238}U and ^{226}Ra are consistent, as shown in Figure 5. However, there are two higher values of ^{238}U and ^{226}Ra around Yamalike Mountain, where uranium mineralization has been found during geological exploration of uranium deposits;
2. ^{137}Cs radionuclides were detected in 30 out of 45 soil samples, but their specific activity varied widely. The average specific activity of ^{137}Cs is 4.42 ± 5.83 Bq/kg, with a maximum of 26.74 Bq/kg. This suggests that 80% of the soil sampling sites were located in relatively undisturbed natural soil layers;

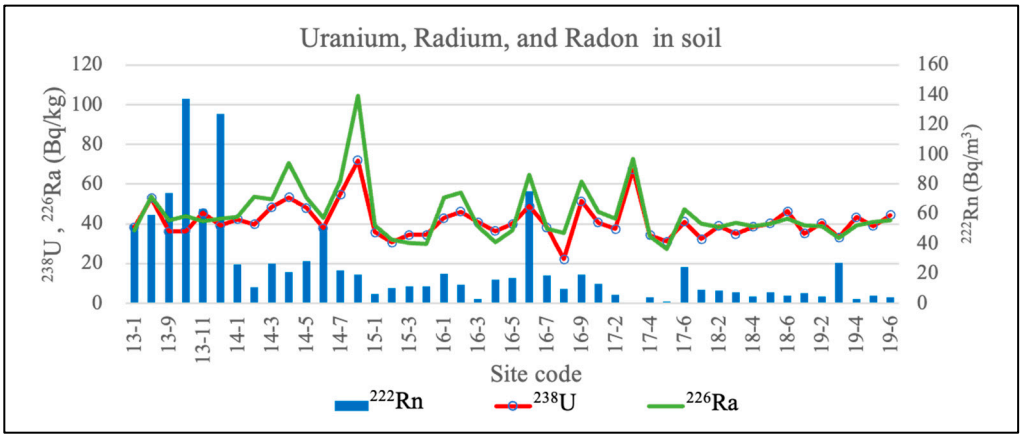

Figure 5. Radon concentration and specific activity of uranium and radium in soil.

3.3. Distribution and Characteristics of Radon in Soil Gas

Measurements of the radon in the soil gas were taken at 68 sites in Urumqi using a RAD7 radon detector, and soil samples were collected at 45 sites. The statistical results of the data for 65 soil radon measurements, after removing three anomalies, are shown in Table 5. Among the three anomalies, two high-value anomalies (137.00 kBq/m^3 and 126.83 kBq/m^3)

are located in a garden near Zhizhu Hill, where the unconformity contact between the Lower Jurassic Karaza Formation and the overlying Upper Cretaceous Qingshuihe Formation is located, and there are a few faults nearby (D2 in Figure 1). One low-value anomaly (268 Bq/m^3) was measured on the side of Yamalike Mountain. Due to the thin topsoil layer in this site, the measured result was significantly low, so the value was removed from the statistical data.

Table 5. Statistics of radon concentration in soil gas by RAD7 (kBq/m^3).

District	N	AM	SD	MIN	MAX	MED	GM
Xinshi District	22	37.97	26.06	2.98	86.69	35.68	27.51
Shayibake District	20	16.64	11.73	1.20	51.54	12.53	12.56
Midong District	6	6.92	1.87	4.37	9.00	7.28	6.69
Shuimogou District	17	8.32	9.20	2.69	26.90	5.50	5.95
Total	65	21.90	20.51	1.20	86.69	15.54	14.57

The statistical parameters of the whole sample are listed in Table 5 and show that the radon in the soil gas is unevenly distributed and the data are highly dispersed, but that their median and GM values are close to each other. The maximum value (86.69 kBq/m^3) was observed in region D2, which was near the high-value anomaly sites. The areas with higher soil radon concentrations appeared in the areas near Zhizhu Hill (D2) in Xinshi District, and Yamalike Mountain (D1) in Shayibake District. A lower radon concentration in the soil gas was observed in Midong District located in northern Urumqi. Areas with low concentrations of soil radon basically correspond to regions with low indoor radon potential, covered with Quaternary sediment.

3.4. Radon Indoor and Gamma Absorbed Dose Rate

Indoor radioactivity levels were investigated using a portable gamma-ray spectrometer in 17 dwellings where instantaneous and long-term cumulative radon comparative measurements were taken. The measured dwellings were all built after 2000. The measured results of the uranium, thorium, and potassium, the absorbed dose rate, and the radon concentration at 17 comparison points (five basements) are shown in Figure 6. It is evident from Figure 6 that the variation in the uranium, thorium, and potassium levels and absorbed dose rate is small, while the radon concentrations change drastically.

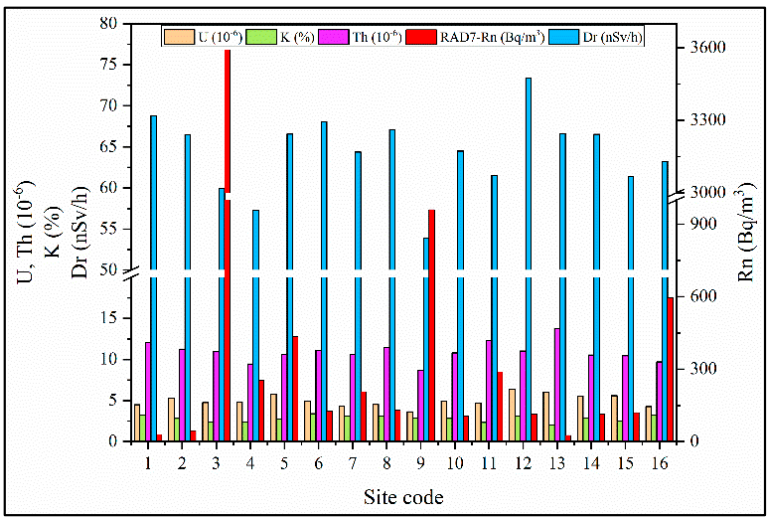

Figure 6. Measured results of Rn, U, Th, K, and dose rate.

It is important to note that the uranium, thorium, and potassium contents determined by the in situ gamma-ray spectrometry are not the result of the quantitative analysis

of radionuclides in building materials, but rather a screening of indoor environmental radioactive levels. This illustrates that the monitored residences did not exhibit elevated levels of radioactive substances. It can be inferred that the indoor radon anomalies were not mainly caused by radionuclides in the building materials in these houses.

4. Discussion

Research data from both domestic and international studies indicate that areas with enriched uranium in the surface soil are generally associated with high indoor radon potential, such as the uranium deposit regions in Utah and Colorado in the United States, in the Czech Republic, and in China [44–46]. Areas characterized by extensive outcrops of acidic granite and the enrichment of heavy sand minerals, such as in Portugal and in Yangjiang and Zhuhai in China, also exhibit elevated uranium content as well as indoor radon levels [11,47–50].

Consequently, some countries in Europe have adopted parameters involving radon concentration in soil gas and soil permeability to study radon potential maps or to use lithological characteristics and geologic structure data to compile radon potential maps. For example, in the "10-point" method of estimating soil radon potential, lithology and faults are important parameters [51].

Our data reveal a uniform distribution of uranium and radium elements in various rocks and soils in Urumqi, with notably low content levels. However, our survey results indicate that 2.8% of the total surveyed buildings exhibited indoor radon concentrations exceeding 400 Bq/m^3. The AM values of the indoor and basement radon concentrations, measured using the SSNTD method by Wang, were 67 ± 40 Bq/m^3, 142 ± 178 Bq/m^3, with a range of 24–499 and 50–775 Bq/m^3, respectively [52]. The number of rooms with indoor radon concentrations higher than 400 Bq/m^3 accounted for 0.7% of all the homes surveyed [52], which was basically consistent with our survey results (Table 1). Notably, anomalies with indoor radon concentrations higher than 3000 Bq/m^3 are found near the Yamalike Fault zone. In this study, the anomalous indoor radon and soil radon identified are mainly located on the northern and southern flanks of the Yamalike anticline, influenced by the Yamalike Fault. Significant variations of radon concentrations were also observed in basements near Zhizhu Hill. In areas where the soil uranium content is similar to that of Urumqi, such as Beijing and Shijiazhuang, the average indoor radon concentration is merely 30 Bq/m^3 [53]. Obviously, the high indoor radon concentration in Urumqi exhibits a weak correlation with the specific activity of radium in soil, because the average specific activity of radium is very low (45 ± 14.1 Bq/kg).

As we know, indoor radon on the first floor of a building generally comes from soil and building materials, while indoor radon levels in high-rise buildings are mainly related to the content of radioactive elements in the building materials. The average specific activities of radium and thorium in the buildings studied in Urumqi were 48.0 and 32.5 Bq/kg, respectively. Only a few cement samples exhibited radium specific activity exceeding the limit value (200 Bq/kg), with the maximum value reaching 230 Bq/kg [52]. The indoor gamma spectrometry data we obtained showed that both the dose rate and uranium specific activity remained stable, even in the presence of variations in the indoor radon concentrations (Figure 6). These results indicate that the indoor radon concentrations should be within the normal range if not supplemented by external radon sources.

The measured soil radon concentration in Urumqi (21.90 kBq/m^3) is lower, ranging from 1.20 to 86.69 kBq/m^3 (Table 5), and the estimated results did not contribute much to the indoor radon concentration. However, the possibility exists that dynamic force could transport radon from deep sources into the room through loose soil and underground cracks. This continuous influx of radon could result in elevated indoor radon concentrations. We speculate that earthquakes might act as such a driving force, and that earthquake events may be one of the potential reasons for the high indoor radon potential in Urumqi.

Strong earthquake waves can induce alterations not only in underground water radon concentration but also in soil radon concentration [54–57]. The region of Urumqi and its

vicinity are recognized for numerous active faults, complex fault interactions, and intense tectonic activity, rendering them prone to recurrent moderate to strong earthquakes [38]. From 1 January to 31 October 2020, Xinjiang experienced a total of 189 earthquakes of M3.0 and above M3.0, including two earthquakes of magnitude 6.0 to 6.9 [58,59]. Focal mechanism solutions by both the United States Geological Survey (USGS) and the China Earthquake Networks Center (CENC) revealed that the M6.0 earthquake in Kashi, Xinjiang, was linked to thrust fault activity [54]. Woith reviewed more than 100 articles on the topic "Radon earthquake precursor" and concluded that "significant radon anomalies exist" and that "seismic-tectonically induced radon anomalies probably exist", while acknowledging that "radon anomalies of non-tectonic origin exist" [60].

It seems that the frequent seismic activity around Urumqi provides the driving force for underground radon's upward migration to the surface. Under the action of frequent medium–strong seismic waves, radon from deep underground migrates to the shallow surface under the action of pressure differences. Due to the high permeability of the soil, combined with the influence of indoor and outdoor temperature differences, the radon from deep underground areas quickly enters the room, thereby elevating the indoor radon concentration. According to the model established by Scott, cracks in the bedrock, fractures in the soil, and cracks in the foundations are the direct reasons for the high rate of radon entering buildings and lead to the high indoor radon concentration in these buildings [61]. Therefore, the high radon potential areas within our survey mainly appeared in areas where there are deep and large faults or overlapping and intersecting zones of multiple groups of faults, such as near Yamalike Mountain and the Jiujiawan Fault Group (Zhizhu Hill).

Moreover, although the results of this study show that the spatial distribution of high radon in indoor areas is correlated with the location of faults, more in-depth and detailed studies are needed to reveal the potential causes of the high radon potential in Urumqi.

5. Conclusions and Suggestions

5.1. Conclusions

In conclusion, based on our indoor instantaneous and long-term radon measurements, soil radon measurements, and radioactive activity analysis of uranium, radium, thorium, and potassium-40 in soil samples in representative areas of Urumqi, we have drawn the following conclusions:

1. The average indoor radon concentration in Urumqi was higher than the national average. Indoor radon concentration in Urumqi is 80 $\pm$ 77 Bq/m^3 for AM and 58 Bq/m^3 for GM, ranging from 9 to 435 Bq/m^3. The AM in the basements is 3.7 times higher than in the houses. There is no relationship between high and abnormal indoor radon concentrations and the buildings' age and construction type. The number of houses with indoor radon concentrations exceeding the standard limit of China's "indoor air quality" standard GB/18883-2022 accounted for 2.8%;
2. The distribution of areas with high indoor radon concentrations is spatially consistent with deep and large faults or overlapping and intersecting zones of multiple groups of faults. Indoor radon anomalies are found near the Yamalike Fault zone and Zhizhu Hill. The high radon potential of the basements and indoor radon is related to fault development, and its wide range may be related to frequent earthquake activities in Xinjiang;
3. The uranium and radium elements in various soils are evenly distributed and their AMs are 41 $\pm$ 9 Bq/kg and 45 $\pm$ 14.1 Bq/kg, respectively;
4. The distribution of radon concentration in the soil is related to faults and lithology. The average radon concentration in the soil is low (21.90 $\pm$ 20.51 Bq/m^3). One of the reasons for the low concentration of radon in the soil is that the surface soil is scoured by snow water, and the content of the fine components of soil in mountainous terrain areas is low, so it is difficult for soil radon to be preserved. The distribution of radon in the soil gas is uneven and the data are highly dispersed.

5.2. Suggestions

Due to the complex geological structure and topography of Urumqi, it is recommended to study the high radon potential, indoor radon characteristics, and radioactivity of building materials in more detail.

Supplementary Materials: The following supporting information can be downloaded at: https://www.mdpi.com/article/10.3390/atmos14101548/s1.

Author Contributions: Conceptualization, N.W.; methodology, N.W. and J.Y. software, H.W.; validation, N.W., H.W. and B.J.; formal analysis, H.W., N.W. and J.Y.; investigation, H.W. and B.J; resources, J.Y.; data curation, H.W. and B.J.; writing—original draft preparation, N.W. and J.Y.; writing—review and editing, N.W. and A.P.; visualization, H.W.; project administration, N.W.; funding acquisition, N.W. All authors have read and agreed to the published version of the manuscript.

Funding: This research was funded by the National Natural Science Foundation of China, grant number 41974167.

Institutional Review Board Statement: The study did not require ethical approval.

Informed Consent Statement: Not applicable.

Data Availability Statement: The data presented in this study were uploaded as a Supplementary File.

Acknowledgments: The authors would like to thank Yunyun Wu, Institute of Radiation Protection and Nuclear Safety Medicine, Chinese Center for Disease Control and Prevention, for her assistance in conducting indoor radon measurements using solid state nuclear tracks detector. We are grateful for the comments and suggestions made by the anonymous reviewers and the academic editor. Thanks to Ying Jiang, a postgraduate student at China University of Geosciences (Beijing) for determining the specific activity of uranium and radium in the soil samples.

Conflicts of Interest: The authors declare no conflict of interest.

References

1. UNSCEAR. *Sources and Effects of Ionizing Radiation, United Nations Scientific Committee on the Effects of Atomic Radiation*; UNSCEAR 2000 report to the general assembly, with scientific annexes, Volume I: Sources; United Nations: New York, NY, USA, 2000.
2. UNSCEAR. *Sources to Effects Assessment for Radon in Homes and Workplaces*; UNSCEAR 2006 report to the general assembly, with scientific annexes, Volume II: Scientific Annexes E; United Nations: New York, NY, USA, 2006.
3. ICRP. *Protection against Radon-222 at Home and at Work*; ICRP Publication 65, Ann. ICRP 23(2); Pergamon Press: Oxford, UK, 1993.
4. Ferlay, J.; Colombet, M.; Soerjomataram, I.; Dyba, T.; Randi, G.; Bettio, M.; Gavin, A.; Visser, O.; Bray, F. Cancer incidence and mortality patterns in Europe: Estimates for 40 countries and 25 major cancers in 2018. *Eur. J. Cancer* **2018**, *103*, 356–387. [CrossRef] [PubMed]
5. Gao, T.; Li, C.; Liang, X.; Zheng, R.; Qiu, T. International Comparison of Cancer Incidence and Mortality in China. *China Cancer* **2016**, *25*, 409–414. (In Chinese) [CrossRef]
6. Åkerblom, G. The use of airborne radiometric and exploration survey data and techniques in radon risk mapping in Sweden. In *Application of Uranium Exploration Data and Techniques in Environmental Studies*; TECDOC-827; IAEA: Vienna, Austria, 1995; pp. 159–180.
7. Keller, G.; Schneiders, H.; Schütz, M.; Siehl, A.; Stamm, R. Indoor radon correlated with soil and subsoil radon potential—A case study. *Environ. Geol. Water Sci.* **1992**, *19*, 113–119. [CrossRef]
8. EPA. *EPA's Map of Radon Zones New York*; USGS Open-file Report 93-292-B; Radon Division Office of Radiation and Indoor Air U.S. Environmental Protection Agency: New York, NY, USA, 1993.
9. EPA. *EPA's Map of Radon Zones Vermont*; EPA-402-R-93-085; Radon Division Office of Radiation and Indoor Air U.S. Environmental Protection Agency: Montpelier, VT, USA, 1993.
10. Alexander, W.; Devocelle, L. Mapping indoor radon potential using geology and soil permeability. In Proceedings of the 1997 International Radon Symposium, Cincinnati, OH, USA, 24–28 August 1997.
11. Wei, L. *High Background Radiation Research in Yangjiang China*; Atomic Energy Press: Beijing, China, 1996.
12. Chen, B.; Guo, Q.; Sun, Q.; Zou, J. Survey on indoor ^{222}Rn, ^{220}Rn progeny in air in high background radiation area of Yangjiang, China. *Radiat. Prot.* **2006**, *26*, 50–55. (In Chinese) [CrossRef]
13. Shang, B.; He, Q.; Wang, Z.; Zhu, C. Studies of indoor action level of radon in China. *Chin. J. Radiol. Med. Prot.* **2003**, *23*, 462–465. (In Chinese) [CrossRef]
14. Wang, N.; Xiao, L.; Li, C. The distribution and level of radon gas in soil in a high radiation background city of China. *Geophys. Geochem. Explor.* **2012**, *36*, 646–650. (In Chinese) [CrossRef]
15. Tang, L.; Zhu, L.; Hu, S.; Liu, Q. Study method on radon geological potential rules. *Rock Miner. Anal.* **1999**, *18*, 3–8. (In Chinese) [CrossRef]

16. Lu, W.; Wang, Z.; Gao, F.; Wang, R. Radon levels in the regional environment of Gejiu, Yunnan, and their relationship to the Geological Features. *Environ. Sci.* **1995**, *16*, 19–23. [CrossRef]
17. Wang, N.; Xiao, L.; Li, C.; Huang, Y.; Pei, S.; Liu, S.; Xie, F.; Cheng, Y. Determination of radioactivity level of ^{238}U, ^{232}Th and ^{40}K in surface medium in Zhuhai City by in-situ Gamma-ray Spectrometry. *J. Nucl. Sci. Technol.* **2005**, *42*, 888–896. [CrossRef]
18. Lei, S.; Tokonami, S.; Sun, Q.; Ishikawa, T.; Kobayashi, Y.; Li, X.; Min, X.; Wu, G.; Yoshinaga, S.; Shang, B. Pilot study on indoor radon and thoron concentrations and terrestrial gamma doses in Gejiu, Yunnan province. *China Occup. Med.* **2008**, *35*, 211–213. (In Chinese) [CrossRef]
19. Shang, B.; Cui, H.; Yang, W. Radon and thoron concentrations in traditional cave dwellings and soil beds. *Radiat. Prot.* **2003**, *23*, 184–188+192. (In Chinese) [CrossRef]
20. Shang, B.; Wang, Z.; Gao, P.; Lei, S. Survey of radon concentrations in cave dwellings in the east of Gansu Province. *Radiat. Prot.* **1995**, *15*, 461–463.
21. Ren, T. Source, level and control of indoor radon. *Radiat. Prot.* **2001**, *21*, 291–299. (In Chinese)
22. The Writing Group of the Summary Report on Nationwide Survey of Environmental Radioactivity Level in China. Survey of concentrations of radon and α potential energy of Rn daughter products in air in some regions of China (1983–1990). *Radiat. Prot.* **1992**, *12*, 164–171. (In Chinese)
23. Xu, D.; Shang, B.; Cao, Z. Investigation of key indoor air pollutants in residence in part of the cities in China. *J. Hyg. Res.* **2007**, *36*, 473–476. (In Chinese) [CrossRef]
24. Shang, B.; Cui, H.; Zhang, L.; Chen, B.; Wu, J.; Wang, Y.; Gao, Y.; Chen, H.; Li, Z.; Wang, M.Z.; et al. Investigation of indoor radon concentration in a typical area of China by solid tracer method. In Proceedings of the Eighth National Conference on Solid State Nuclear Tracing, Xiamen, China, 15–19 October 2004; Chinese Society of Nuclear Physics: Beijing, China, 2004.
25. Wang, C.; Pan, Z.; Liu, S.; Yang, M.; Shang, B.; Zhuo, W.; Ren, T.; Xiao, D.; Yang, W.; Li, F.; et al. Investigation on indoor radon levels in some parts of China. *Radiat. Prot.* **2014**, *34*, 65–73. (In Chinese)
26. Zhu, W.; Lin, J.; Li, Z.; Lei, S.; Sun, X.; Liu, F. Investigation on radon concentration in Urumqi metro line 1. *Bull. Dis. Control Prev. China* **2021**, *36*, 59–60+72. (In Chinese) [CrossRef]
27. Wang, X.; Jin, Y.; Chen, Z.; Zhuo, W.; Zhu, L. *China Indoor Radon Study*; Science Press: Beijing, China, 2013. (In Chinese)
28. Han, Q.; Lv, A.; Su, J. Reinvestigation on influence parameters of indoor radon concentration in Urumqi and relevant countermeasures. *Radiat. Prot.* **2012**, *32*, 171–176+192. (In Chinese)
29. Tu, Q.; Xie, N.; Wei, Z.; Liu, Z.; Zhang, X.; Wei, Q.; Wang, X.; Li, Y.; Lei, Y. *The Report of the 1/250,000 Multi-Target Regional Geochemical Survey in Urumqi-Changji Area*; National Geological Library: Beijing, China, 2011. (In Chinese) [CrossRef]
30. Su, J.; Xu, M.; Li, M.; Guo, Y.; Han, Q. Investigation on soil radon concentration levels and distribution in Urumqi. *Radiat. Prot.* **2009**, *29*, 327–333. (In Chinese)
31. *GB/T 18883-2022*; Standard of Indoor Air Quality. State Administration for Market Regulation and National Standardization Administration. Standards Press of China: Beijing, China, 2022. (In Chinese)
32. Wang, N.; Peng, A.; Xiao, L.; Chu, X.; Yin, Y.; Qing, C.; Zheng, L. The level and distribution of ^{220}Rn concentration in soil-gas in Guangdong Province, China. *Radiat. Prot. Dosim.* **2012**, *152*, 204–209. [CrossRef]
33. Wang, N.; Zheng, L.; Chu, X.; Li, S.; Yan, S. The characteristics of radon and thoron concentration from soil gas in Shenzhen City of Southern China. *Nukleonika* **2016**, *61*, 315–319. [CrossRef]
34. Wu, Y.; Cui, H.; Zhang, Q.; Shang, B. Intercomparisons for integrating the radon–thoron detector of NIRP, China with NIRS, Japan. *Radiat. Prot. Dosim.* **2015**, *164*, 398–401. [CrossRef] [PubMed]
35. *GB/T 16145-2022*; Gamma-Ray Spectrometry Method for the Determination of Radionuclides in Environmental and Biological Samples. State Administration for Market Regulation of the People's Republic of China, Standardization Administration of the People's Republic of China, Standards Press of China: Beijing, China, 2022. (In Chinese)
36. Urumqi Municipal People's Government. Overview of Urumqi. Available online: http://www.urumqi.gov.cn/wlmjgk/447021.htm (accessed on 5 June 2023).
37. Waheiti, W.; Ren, G.; Sun, X. The daily temperature characteristics of the intensity of urban heat island in Urumqi and seasonal changes. *Desert Oasis Meteorol.* **2018**, *12*, 21–28.
38. Zhang, H.; Xie, F.; Cui, X.; Du, Y.; Shu, S. Active fault sliding and recent tectonic stress field in the Urumqi area. *Earthq. Res. China* **2006**, *22*, 259–268. (In Chinese) [CrossRef]
39. Ye, M.; Su, N. Active faults and urban construction. *City Disas. Reduc.* **2004**, *4*, 13–16. (In Chinese) [CrossRef]
40. Yang, F. The geologic structure and earthquake movement in the area of Urumqi. *J. Xinjiang Norm. Univ. Nat. Sci. Ed.* **1990**, *2*, 84–89. (In Chinese)
41. Tang, L.; Shen, J.; Liu, Z. Determination of potential seismic source in Urumqi region and its periphery. *Inland Earthq.* **2010**, *24*, 8–12. (In Chinese) [CrossRef]
42. Wu, Y.; Song, Y.; Zhang, Q.; Shang, B.; Cui, H.; Hou, C. Indoor radon concentration and its changing trend in northeastern China. *Chin. J. Radiol. Health* **2023**, *32*, 115–118+130. (In Chinese)
43. Shang, B.; Cui, H.; Wu, J.; Zhang, L.; Chen, B. Study on indoor radon level and its influencing factors in China. In Proceedings of the 2nd National Symposium on Natural Radiation Exposure and Control, Beijing, China, 5 December 2005. (In Chinese).
44. Cui, L. Radiometric methods in regional radon hazard mapping. *Geophys. Geochem. Explor. Abroad* **1991**, *4*, 18–24. (In Chinese)
45. Cui, L. Some results of radon hazard investigations. *Geol. Rev.* **1994**, *40*, 157–164. (In Chinese) [CrossRef]

46. Gan, N.; Cen, K.; Ye, R.; Li, T. Rapid estimation of environmental radioactivity surrounding Xiangshan uranium deposits, Jiangxi province, Eastern China. *Nukleonika* **2018**, *63*, 113–121. [CrossRef]
47. Carvalho, F.P.; Madruga, M.J.; Reis, M.C.; Alves, J.G.; Oliveira, J.M.; Gouveia, J.; Silva, L. Radioactivity in the environment around past radium and uranium mining sites of Portugal. *J. Environ. Radioact.* **2007**, *96*, 39–46. [CrossRef] [PubMed]
48. Yuan, Y.; Morishima, H.; Shen, H.; Mioko, K.; Wei, L.; Jian, Y. Estimation of doses to the residents arising from inhalation of Rn-222, Rn-220 and their decay products in high background radiation area of Yangjiang. *Chin. J. Radiol. Health* **2002**, *11*, 65–68. (In Chinese) [CrossRef]
49. Guo, Q.; Cheng, J. Measurement of ^{222}Rn/^{220}Rn progeny and exhalation rates for ^{222}Rn/^{220}Rn from soil in Zhuhai area. *Radiat. Prot.* **2004**, *24*, 110–115. (In Chinese) [CrossRef]
50. Xiao, L.; Wang, N.; Li, C.; Liu, S.; Huang, Y.; Liu, D. Indoor concentration of ^{222}Rn in Zhuhai typical area. In Proceedings of the Third National Symposium on Natural Radiation Exposure and Control, Baotou, China, 29 August 2010.
51. Bleile, D.; Wiegand, J. Checking the "10 point system" for an evaluation of the soil radon potential. *Radioact. Environ.* **2005**, *7*, 833–841. [CrossRef]
52. Wang, Y. Study and Hygienic Evaluation on Indoor and Outdoor Radon Concentration in Part Area of Xinjiang. Master's Thesis, Xinjiang Medical University, Xinjiang, China, 2003.
53. Qin, C.; Wang, N.; Xiao, L.; Chu, X. The correlation between indoor radon concentrations and geological backgrounds in some typical areas of Beijing and Guangdong. *Geophys. Geochem. Explor.* **2012**, *36*, 441–444. [CrossRef]
54. Yao, Y.; Li, T.; Liu, Q.; Di, N. Characteristics of geological hazards in the epicenter of the Jiashi M_W6.0 earthquake on January 19, 2020. *Seismol. Geol.* **2021**, *2*, 410–429. (In Chinese) [CrossRef]
55. Alam, A.; Wang, N.; Zhao, G.; Barkat, A. Implication of Radon Monitoring for Earthquake Surveillance Using Statistical Techniques: A Case Study of Wenchuan Earthquake. *Geofluids* **2020**, *2020*, 2429165. [CrossRef]
56. Alam, A.; Wang, N.; Petrak, E.; Barkat, A.; Huang, F.; Shah, M.A.; Cantzos, D.; Priniotakis, G.; Yannakopoulos, P.H.; Papoutsidakis, M.; et al. Fluctuation Dynamics of Radon in Groundwater Prior to the Gansu Earthquake, China (22 July 2013: M_s = 6.6): Investigation with DFA and MFDFA Methods. *Pure Appl. Geophys.* **2021**, *178*, 3375–3395. [CrossRef]
57. Du, J.; Yu, W.; Li, S.; Jian, C.; Zhu, Z.; Chen, H.; Kang, C. The geochemical characteristics of escaped radon from the Babaoshan fault zone and its earthquake reflecting effect. *Earthquake* **1998**, *18*, 155–162. (In Chinese)
58. New Beijing News. In the First 10 Months of This Year, 513 Earthquakes of Magnitude 3 or Higher Occurred in China. Available online: https://news.sina.com.cn/c/2020-11-01/doc-iiznezxr9270929.shtml (accessed on 9 February 2023).
59. Guangdong Earthquake Agency. Available online: http://www.gddzj.gov.cn/gddzj/dzpd/yzqgk/714752/index.html (accessed on 6 June 2023).
60. Woith, H. Radon earthquake precursor: A short review. *Eur. Phys. J. Spec. Top.* **2015**, *224*, 611–627. [CrossRef]
61. Scott, A. Radon Sources, Radon Ingress and Models. *Radiat. Prot. Dosim.* **1994**, *56*, 145–149. [CrossRef]